Behavior of Sn atoms in GeSn thin films during thermal annealing: Ex-situ and in-situ observations

Ryohei Takase, Manabu Ishimaru, Noriyuki Uchida, Tatsuro Maeda, Kazuhisa Sato, Ruben R. Lieten, and Jean-Pierre Locquet

Citation: Journal of Applied Physics **120**, 245304 (2016);
View online: https://doi.org/10.1063/1.4973121
View Table of Contents: http://aip.scitation.org/toc/jap/120/24
Published by the American Institute of Physics

Behavior of Sn atoms in GeSn thin films during thermal annealing: *Ex-situ* and *in-situ* observations

Ryohei Takase,[1] Manabu Ishimaru,[1,a)] Noriyuki Uchida,[2] Tatsuro Maeda,[2] Kazuhisa Sato,[3,b)] Ruben R. Lieten,[4,5] and Jean-Pierre Locquet[5]
[1]*Department of Materials Science and Engineering, Kyushu Institute of Technology, Kitakyushu, Fukuoka 804-8550, Japan*
[2]*Nanoelectronics Research Institute, Advance Industrial Science and Technology, Central 5, 1-1-1 Higashi, Tsukuba, Ibaraki 305-8562, Japan*
[3]*Institute for Materials Research, Tohoku University, Sendai, Miyagi 980-8577, Japan*
[4]*IMEC, 3001 Leuven, Belgium*
[5]*Department of Physics and Astronomy, KU Leuven, 3001 Leuven, Belgium*

(Received 21 October 2016; accepted 12 December 2016; published online 30 December 2016)

Thermally induced crystallization processes for amorphous GeSn thin films with Sn concentrations beyond the solubility limit of the *bulk* crystal Ge-Sn binary system have been examined by X-ray photoelectron spectroscopy, grazing incidence X-ray diffraction, and (scanning) transmission electron microscopy. We paid special attention to the behavior of Sn before and after recrystallization. In the as-deposited specimens, Sn atoms were homogeneously distributed in an amorphous matrix. Prior to crystallization, an amorphous-to-amorphous phase transformation associated with the rearrangement of Sn atoms was observed during heat treatment; this transformation is reversible with respect to temperature. Remarkable recrystallization occurred at temperatures above 400 °C, and Sn atoms were ejected from the crystallized GeSn matrix. The segregation of Sn became more pronounced with increasing annealing temperature, and the ejected Sn existed as a liquid phase. It was found that the molten Sn remains as a supercooled liquid below the eutectic temperature of the Ge-Sn binary system during the cooling process, and finally, β-Sn precipitates were formed at ambient temperature. *Published by AIP Publishing.* [http://dx.doi.org/10.1063/1.4973121]

I. INTRODUCTION

Because of its tunable band gap and high carrier mobility, germanium-tin (GeSn) is a promising material for extending the applicable fields of current silicon-based electronic device technologies.[1] In addition, the lattice parameter of the material can be controlled by Sn doping, which is useful for strain engineering applications.[2] Controlling the Sn concentration in a wide range is of technological importance for obtaining desirable material properties. However, the solubility limit of Sn in *bulk* crystalline Ge is very small (~1.1 at. % at 400 °C), according to the phase diagram of the Ge-Sn binary system.[3] Much effort has been devoted to enhancing the Sn concentration incorporated into the Ge matrix. Solid phase recrystallization from the amorphous phase is one of the possible ways to produce Ge containing a large amount of Sn.[4,5] In fact, polycrystalline GeSn thin films with Sn concentrations beyond the solubility limit have been realized using this technique.[6–8]

Polycrystalline GeSn thin films grown on an insulator are anticipated as an alternative to polycrystalline Si films, which are currently utilized as a channel material for thin film transistors (TFTs). Amorphous GeSn recrystallizes at a lower temperature than amorphous Si because of its low eutectic temperature (231.1 °C); consequently, low-temperature fabrication of TFT products can be established. For TFT applications, it is important to enhance thermal conductivity to avoid self-heating[9] and to realize high carrier mobility for fast response. We have recently examined the electrical and thermal properties of polycrystalline GeSn thin films grown on SiO_2 and demonstrated their potential capabilities as a high-performance TFT channel material.[10] We also found that the carrier mobility and density suddenly change between 460 °C and 480 °C. This alteration is strongly correlated with Sn segregation from the matrix; therefore, understanding the Sn behavior during thermal annealing is technologically important for controlling the physical properties of the materials. However, previous studies were performed using *ex-situ* techniques, and direct observations of crystallization processes have never been performed.

In the present study, we examined the structural changes of amorphous GeSn as well as the behavior of Sn during thermal annealing using a variety of characterization techniques. In addition, the Sn behavior at temperatures above the eutectic point of the Ge-Sn binary system was directly observed by *in-situ* transmission electron microscopy (TEM) using a heating holder.

II. EXPERIMENTAL PROCEDURES

Amorphous GeSn thin films with a thickness of ~100 nm were deposited on a sputtered SiO_2/Si substrate at ~10 °C using molecular beam deposition. Ge (99.99%) and Sn (99.99%) were evaporated from separate effusion cells in

a)Author to whom correspondence should be addressed. Electronic mail: ishimaru@post.matsc.kyutech.ac.jp
b)Present address: Research Center for Ultra-High Voltage Electron Microscopy, Osaka University, Ibaraki, Osaka 567-0047, Japan

an ultrahigh vacuum chamber at a base pressure of 2.6×10^{-8} Pa; molecular beam pressures of 2.1×10^{-5} Pa and 3.6×10^{-6} Pa were used for Ge and Sn, respectively. From Rutherford backscattering spectroscopy, the composition of the thin film was estimated to be 13.8 at. %Sn. The as-deposited specimens were annealed via halogen lamp heating at 350–520 °C in N_2 gas for 30 min. The sample preparation techniques are described elsewhere.[10]

The as-deposited and annealed specimens were characterized by X-ray photoelectron spectroscopy (XPS), grazing incidence X-ray diffraction (GIXRD), transmission electron microscopy (TEM), and scanning transmission electron microscopy (STEM). XPS analyses were performed using a Kratos AXIS Ultra DLD. Monochromatic Al-$K\alpha$ X-rays (1486.7 eV) were used to obtain the core level spectra of the specimens. To remove the oxide layer and contamination of the surface, XPS measurements were performed after Ar ion sputtering for 1 min. GIXRD measurements were carried out on a Rigaku SmartLab X-ray diffractometer using Cu-$K\alpha$ radiation at 40 kV and 30 mA, and the incident angle of X-rays was set to $\omega = 0.5°$. Cross-sectional specimens for TEM observations were prepared by a combination of mechanical polishing and ion thinning. TEM observations were performed using a JEOL JEM-3000F, while a JEM-ARM200F was utilized for elemental mapping. Both the facilities were operated at 200 kV.

Amorphous materials are not completely disordered but possess a certain order at the atomic scale, so-called short-range order. The short-range ordered state can be characterized by atomic pair-distribution functions, in which the atomic configurations are described by the probability of finding another atom at a distance between r and $r + dr$ from a specific atom.[11] To obtain atomic pair-distribution functions, a quantitative analysis of electron diffraction intensities is required. In the present study, electron diffraction patterns were recorded on imaging plates and the intensities of the halo rings were digitized quantitatively using an imaging plate processor, DITABIS Micron. The detailed procedures for atomic pair-distribution analysis are described elsewhere.[12–17]

III. RESULTS AND DISCUSSION

A. Structure of as-deposited GeSn thin films

Figure 1(a) shows a cross-sectional bright-field TEM image of the as-deposited GeSn thin film. No remarkable diffraction contrast resulting from crystallites or compositional fluctuation exists in the film. Indeed, halo rings are observed in the electron diffraction pattern taken from the thin film (inset of Fig. 1(a)), and the high-resolution TEM image shows a typical salt-and-pepper contrast (Fig. 1(b)): the as-deposited specimen possesses an amorphous structure. Energy-dispersive X-ray spectroscopy (EDX) analysis of Fig. 1(c) reveals the existence of Sn, and the average Sn composition was estimated to be 10.6 at. %, which is almost comparable to the concentration estimated by Rutherford backscattering spectroscopy. This value is much larger than the solubility limit of Sn in crystalline Ge (~1.1 at. % at 400 °C).[3] The high-angle annular dark-field (HAADF) image

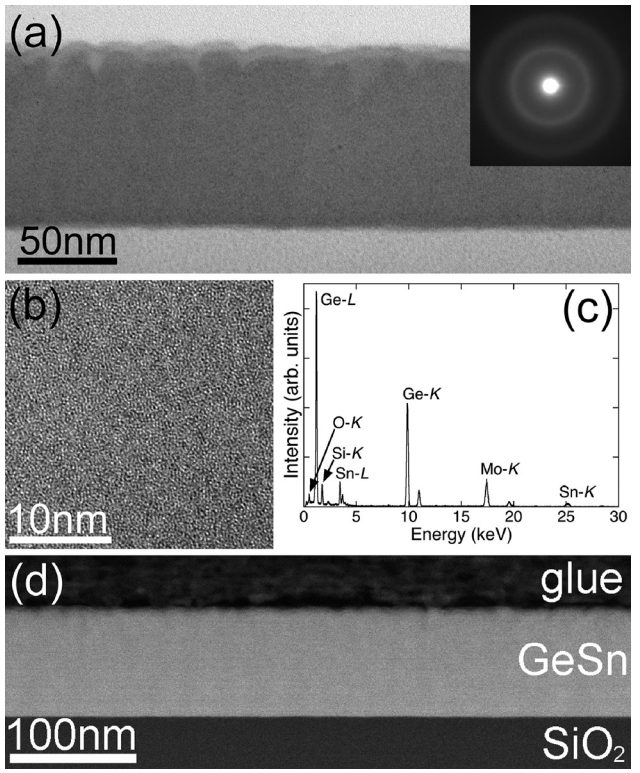

FIG. 1. Cross-sectional observations of as-deposited GeSn thin film on SiO_2. (a) Bright-field TEM images and electron diffraction pattern, (b) high-resolution TEM image, (c) EDX spectrum, and (d) HAADF-STEM image. The diffraction pattern shows halo rings, and the high-resolution TEM image reveals a typical salt-and-pepper contrast, indicating that the as-deposited thin film is amorphous. The Sn concentration estimated by EDX spectra is 10.6 at. %, and the HAADF-STEM image reveals no remarkable phase separation in the specimen. In (c), the peak of molybdenum comes from a molybdenum mesh supporting the TEM specimen.

of Fig. 1(d) shows no contrast fluctuation, except that resulting from the thickness difference along the direction of the incident electron beam. This suggests that Sn atoms are homogeneously distributed in the specimen.

B. Compositional changes during thermal annealing

Figure 2(a) shows the XPS profile of the as-deposited GeSn thin film in the energy range from 0 to 1200 eV. Sn segregation at both the surface and interface became more pronounced with increasing annealing temperature. We confirmed that the surface layer is oxidized, and therefore the XPS spectra were obtained from the inside of the thin film after removing the oxide layer by sputtering. All the peaks are assigned to Sn, Ge, and Auger spectra, and the lack of a peak associated with carbon (e.g., C 1s: 285 eV) suggests no remarkable contamination. The Ge 3*d* and Sn 3*d* core-level XPS spectra obtained from as-deposited specimens and those annealed at 500 °C are shown in Figs. 2(b) and 2(c), respectively. Signals appear at 29.2 eV for Ge 3*d* and 484.9 eV for Sn $3d_{5/2}$, and others resulting from oxidation (i.e., 486.7 eV for SnO_2 and 32.5 eV for GeO_2) are absent (or very weak): pure GeSn thin films were successfully formed in the present study. Similar Sn 3*d* core-level XPS spectra were also reported for high-quality $Ge_{0.83}Sn_{0.17}$ produced by Lei *et al.*[18] Sn concentration as a function of annealing temperature is shown in Fig. 2(d).

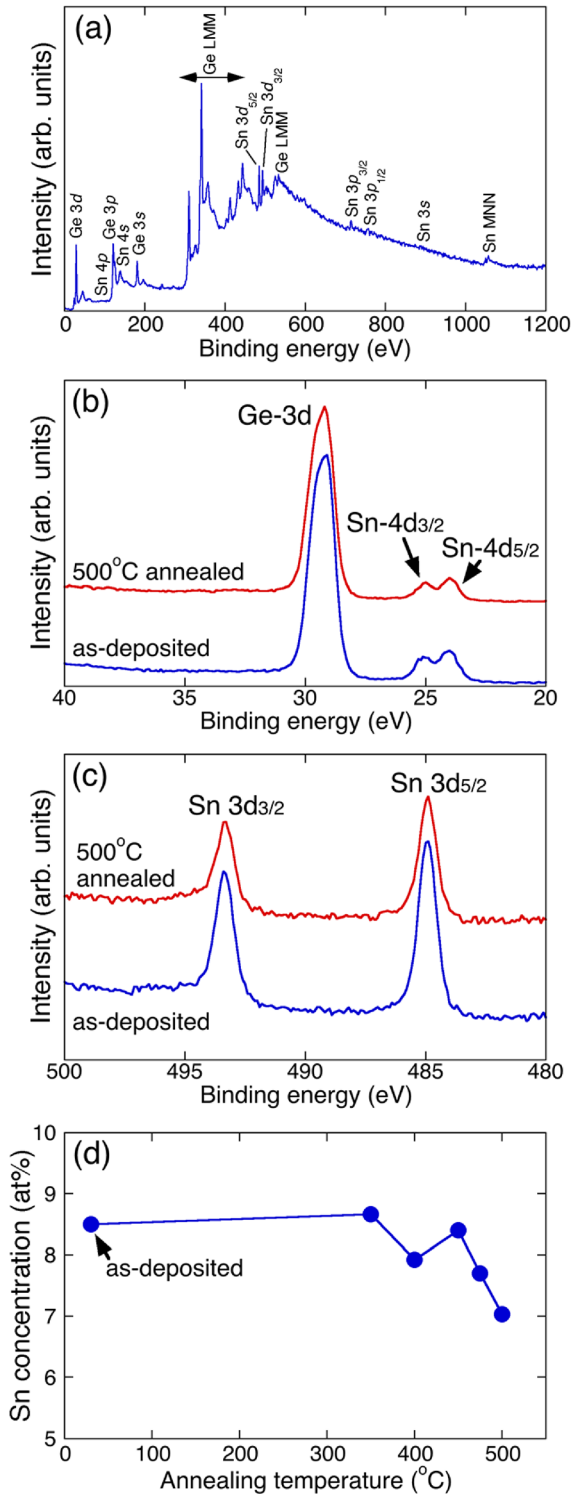

FIG. 2. (a) Overview XPS spectra of the as-deposited GeSn thin film. (b) Core-level XPS spectra of (b) Ge 3*d* and (c) Sn 3*d* obtained from as-deposited GeSn specimens and those annealed at 500 °C. (d) Sn concentration as a function of annealing temperature. Neither remarkable oxidation nor contamination occurs during sample preparation.

The accuracy of atomic concentration estimated by XPS is 5%; therefore, only the qualitative trends can be discussed here. The specimens were annealed above 350 °C for crystallization. This temperature is much higher than the eutectic temperature of the Ge-Sn binary system; therefore, significant reduction of Sn concentration was expected. However, the Sn concentration slightly decreases after thermal annealing, and it was found that most of the Sn atoms remain in the thin films.

Figure 3(a) shows GIXRD profiles obtained from the as-deposited and annealed specimens. Broad peaks from an amorphous structure are observed in the as-deposited specimen, in agreement with TEM results described above. Most of the amorphous structure remains in the specimen annealed at 350 °C, whereas a remarkable crystallization occurs at >400 °C. The strong peaks present at $2\theta = \sim 27°$, $\sim 45°$, and $\sim 53°$ can be indexed to 111, 220, and 311 Bragg reflections of GeSn with a diamond structure, as reported previously.[10] The magnified profiles around the 111 reflection are shown in Fig. 3(b). Because of the improvement of the crystallinity and the increase in the crystal size, the peaks become sharper with increasing annealing temperature. The peak position shifts to the higher-angle side with thermal annealing, indicating a reduction of the lattice constant. The inset of Fig. 3(a) shows the lattice parameter obtained from the different Bragg peaks. The values extracted from the 111, 220, and 311 reflections are not consistent, suggesting the existence of lattice distortion in GeSn. The distortion decreases with increasing annealing temperature. The lattice contrast estimated from the 111 peak location is as follows: 0.577 nm for specimens annealed at 400 °C, 0.574 nm for 450 °C, 0.572 nm for 475 °C, and 0.568 nm for 500 °C.[10] These values are larger than that of Ge (0.5658 nm), suggesting the incorporation of Sn into the Ge matrix. The reduction of the lattice constant with increasing annealing temperature suggests the ejection of Sn atoms from Ge. In the diamond structure, planar defects are preferentially introduced on the (111) plane. In this case, the spacing of the (111) planes is maintained as compared to other planes; therefore, we estimated the substitutional Sn concentration using the 111 reflection.

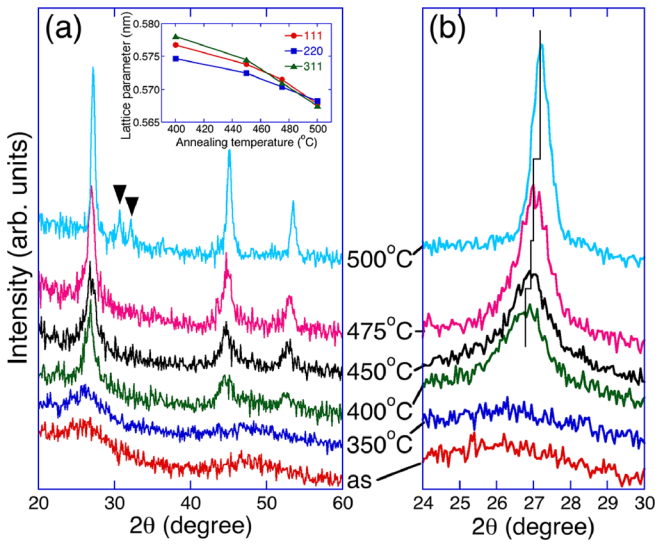

FIG. 3. GIXRD profiles of the crystallized GeSn thin films as a function of annealing temperature. (a) Overview profiles ranging from $2\theta = 28°$ to 65° and (b) magnified image of the 111 reflection. Strong peaks are indexed to 111, 220, and 311 Bragg reflections of GeSn with a diamond structure. In addition to these peaks, peaks from β-Sn marked by triangles are observed in the profile of GeSn annealed at 500 °C. The peaks of GeSn become narrow and shift to the higher angle side with increasing annealing temperature. The lattice parameters estimated from the 111, 220, and 311 reflections are shown as an inset in (a).

The resultant values are as follows: 13 at. %Sn for 400 °C, 10 at.%Sn for 450 °C, 7 at. %Sn for 450 °C, and 3 at. %Sn for 500 °C. Here, Vegard's law was applied, and the lattice parameters of Ge and α-Sn are assumed to be 0.5658 nm and 0.6493 nm, respectively. Although the Sn concentration estimated here includes some errors because of the deviation from Vegard's law,[19] it was confirmed that our crystallized GeSn thin films possess a Sn concentration beyond the solubility limit of the *bulk* Ge-Sn binary system. Based on the density functional theory, it has been reported that vacancies are preferentially trapped with Sn atoms in Ge.[20–23] In general, amorphous materials contain free volumes,[24–26] which presumably causes the Sn-vacancy pairs. As a consequence, substitutional Sn atoms, with a concentration that is much higher than the solubility limit, are stabilized in the crystalline Ge matrix.

C. Structural changes during thermal annealing

The structural evolution of GeSn thin films during thermal annealing was examined by cross-sectional TEM. Figure 4 shows a series of bright-field images of GeSn as a function of annealing temperature. From the diffraction contrast, it was found that some crystallization occurs at 350 °C (Fig. 4(a)), which is much lower than the crystallization temperature of amorphous Ge.[27] The grain size increases with thermal annealing (Fig. 4(b), and, finally, the formation of voids between the thin film and substrate is observed (Fig. 4(c)). (The detailed structural changes in GeSn have been reported in our previous study.[10]) In addition to the reflections associated with GeSn with a diamond structure, some spots resulting from segregated Sn (marked with arrows) are observed in the diffraction pattern of Fig. 4(c). High-resolution TEM observations and nano-beam electron diffraction experiments reveal the formation of β-Sn (Fig. 5). Indeed, the Bragg reflections associated with Sn precipitates are observed at $2\theta = \sim 31°$ and $\sim 32°$ (marked with triangles in Fig. 3(a)) in the GIXRD profile of GeSn annealed at 500 °C. As described above, the present specimens contain Sn atoms beyond the solubility limit of

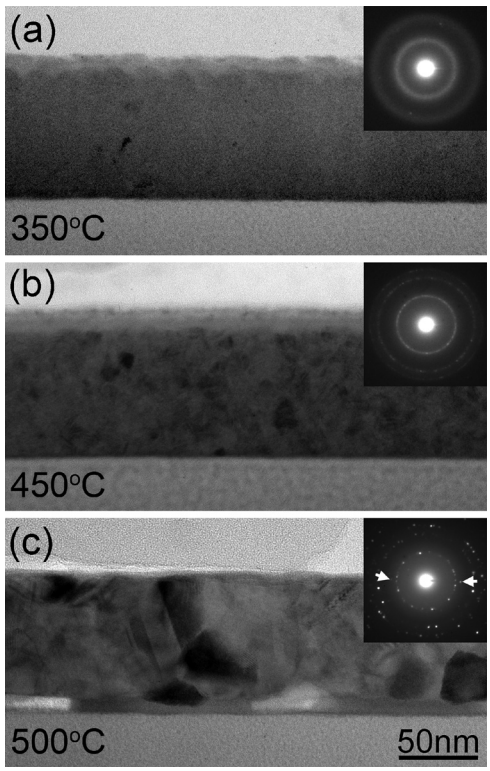

FIG. 4. Structural evolution of GeSn thin films during thermal annealing: (a) 350 °C, (b) 450 °C, and (c) 500 °C. Slight recrystallization is observed in (a), and the grain size increases with thermal annealing. Bragg spots from β-Sn indicated by arrows appear in the electron diffraction pattern of (c).

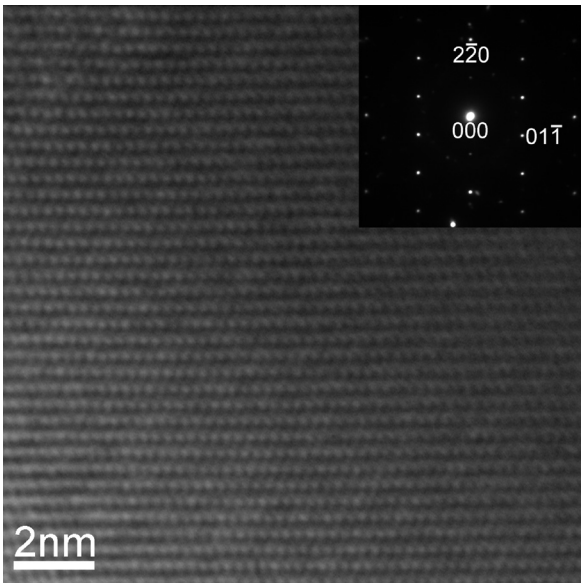

FIG. 5. High-resolution TEM image and electron diffraction pattern obtained from a grain of GeSn annealed at 500 °C. The atomic arrangement and diffraction pattern are in agreement with those of β-Sn viewed along the [111] direction.

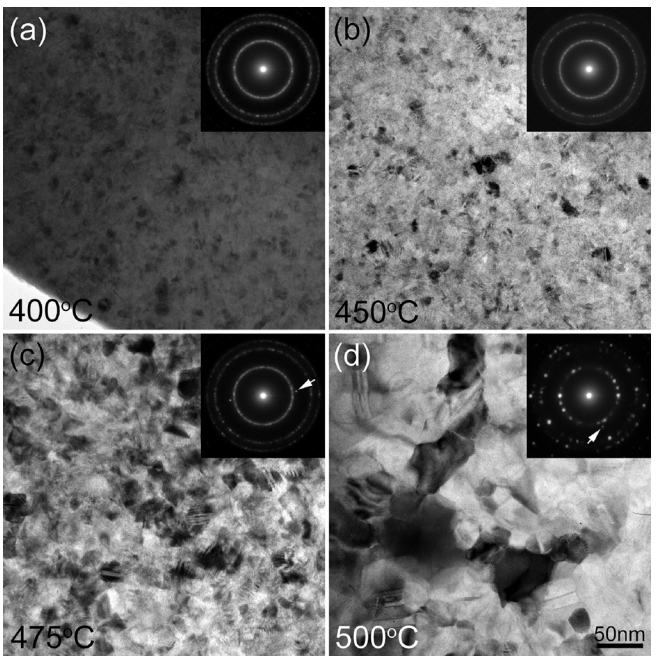

FIG. 6. Plane-view bright-field TEM images and electron diffraction patterns taken at various annealing temperatures: (a) 400 °C, (b) 450 °C, (c) 475 °C, and (d) 500 °C. In addition to the rings from GeSn with a diamond structure, the reflections of β-Sn marked with arrows exist in the diffraction patterns of (c) and (d).

crystalline Ge. The excess Sn atoms are ejected from the matrix with thermal annealing; consequently, the lattice parameter decreases.

Figure 6 shows plane-view bright-field TEM images of the specimens obtained at various annealing temperatures. Diffraction contrast caused by grains is observed, and their size increases with thermal annealing. Again, it was confirmed that the spots of crystalline Sn, marked with arrows, appear in the specimens annealed at 475 °C (Fig. 6(c)) and 500 °C (Fig. 6(d)). It should be noted that the Sn crystallites were not detected at 475 °C in our previous cross-sectional TEM observations.[10] The diffraction patterns were taken from a wider region in plane-view specimens than in cross-sectional ones; therefore, a small amount of Sn crystallites is successfully detected in the present study. The bright-field images above 475 °C contain Sn grains. To estimate the grain size of GeSn only, plane-view dark-field TEM observations were performed. Figure 7 shows dark-field images taken using the 111 reflection of GeSn. The GeSn grains are clearly observed as the bright contrast. The inset is the histogram of the grain size extracted from the dark-field image. Grain growth apparently occurs with increasing annealing temperature. The average grain sizes are as follows: 10 nm for 400 °C, 12 nm for 450 °C, 17 nm for 475 °C, and 39 nm for 500 °C.

To obtain information on the spatial distribution of Sn, we performed HAADF-STEM observations and elemental mapping of the GeSn thin film using STEM. Figure 8 shows HAADF-STEM images and elemental maps of the crystallized specimens at ((a)–(c)) 400 °C, ((d)–(f)) 475 °C, and ((g)–(i)) 500 °C. The specimen annealed at 400 °C shows a homogeneous contrast in the HAADF-STEM image of Fig. 8(a), but a closer examination reveals a contrast fluctuation (see the inset). The contrast of the HAADF-STEM image is proportional to the square of the atomic number; therefore, the contrast is presumably due to compositional fluctuation. It is thought that the Sn-rich region acts as a nucleation site for crystallites, and as a consequence, the crystallization temperature becomes lower than that of amorphous Ge. The elemental maps taken by the characteristic X-rays of Ge-*L* and Sn-*L* lines reveal uniform elemental distribution (Figs. 8(b) and 8(c)) because of their lower detection efficiency than HAADF. Similar elemental maps are obtained for the specimen annealed at 475 °C (Figs. 8(e) and 8(f)), but the bright contrast from Sn precipitates is clearly observed in the HAADF-STEM image of Fig. 8(d). It should be noted that the Sn concentration becomes more pronounced at the interface between the thin film and substrate. This is attributed to the slight reduction in Sn concentration with thermal annealing, as detected by XPS analysis (Fig. 2(d)). A similar segregation of Sn was also observed in GeSn thin films grown on Si.[28] Finally, a remarkable phase separation is detected in specimens annealed at 500 °C by the HAADF-STEM image and elemental mapping (Figs. 8(g)–8(i)). We have recently found that the Hall carrier mobility and concentration of polycrystalline GeSn suddenly change between 460 and 480 °C.[10] On the basis of the HAADF-STEM and elemental mapping results, this issue can be attributed to the remarkable segregation of Sn atoms in the GeSn matrix. The bright

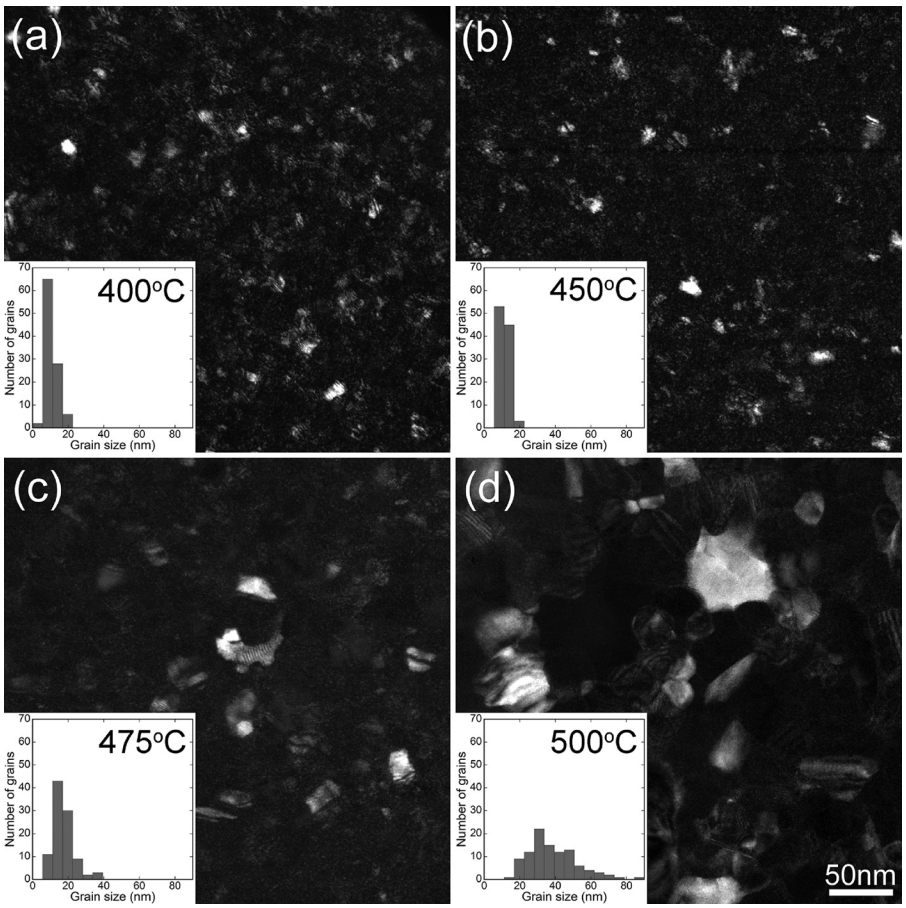

FIG. 7. Plane-view dark-field TEM images and histograms of grain size as a function of annealing temperature. The 111 reflection of GeSn was used for imaging. It is apparent that the grain size increases with thermal annealing.

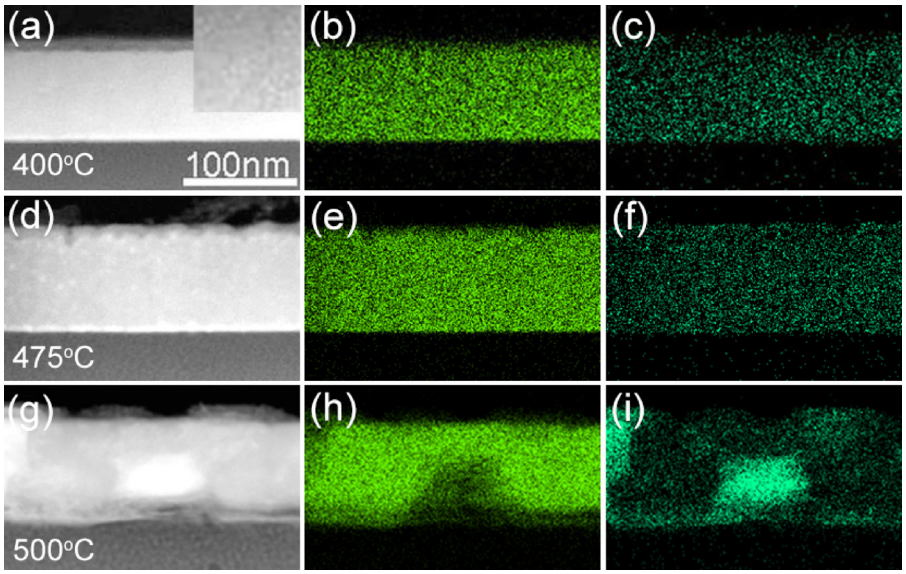

FIG. 8. HAADF-STEM images and elemental maps of GeSn annealed at the following temperatures: ((a)–(c)) 400 °C, ((d)–(f)) 475 °C, and ((g)–(i)) 500 °C. For the elemental mapping, the characteristic X-rays of Ge-*L* and Sn-*L* were used. It is apparent that the Sn segregation occurs at 475 °C and becomes more pronounced with increasing annealing temperature.

contrast arising as a result of Sn segregation at the interface becomes faint in Fig. 8(g). We confirmed that Sn atoms react with Ge and O at the interface with increasing annealing temperature, which presumably contributes to the disappearance of the contrast at the interface.

D. *In-situ* observations of structural changes

The eutectic temperature of the Ge-Sn binary system is 231.1 °C. Therefore, it is expected that the specimens are partially melted under the present annealing conditions. To clarify the behavior of Sn atoms, the annealing processes of GeSn thin films were examined by *in-situ* TEM. Figure 9 shows the structural changes in GeSn during the heating process. From the diffraction contrast in the bright-field image and diffraction spots in the diffraction pattern, it was judged that the amorphous GeSn thin film starts to crystallize at 350 °C (Fig. 9(a)), in good agreement with *ex-situ* observations of Fig. 4(a). A ring pattern caused by crystallization appears in the selected-area electron diffraction pattern of Fig. 9(b), and the rings can be indexed to 111, 220, and 311 Bragg reflections of GeSn with a diamond structure. Note that extra spots inside the first ring and between the first and second rings are due to contamination during *in-situ* observations and therefore should be ignored. Further thermal annealing induces grain growth, which is evident from the discontinuity of rings in the diffraction pattern of Fig. 9(c). In addition to the strong spots caused by GeSn crystallites, a diffuse ring indicated by an arc can be observed in specimens annealed at 500 °C, suggesting the existence of a liquid phase. No apparent Bragg spots from crystalline Sn are observed in the diffraction patterns, suggesting that all the segregated Sn exists as a liquid phase.

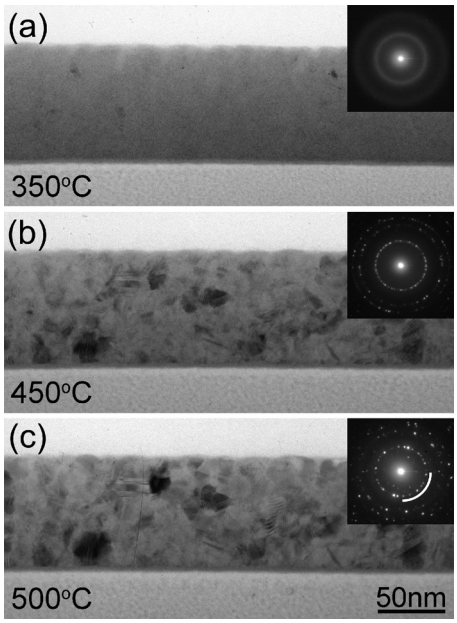

FIG. 9. *In-situ* TEM observations on structural evolution of GeSn during the heating process. (a) 350 °C, (b) 450 °C, and (c) 500 °C. The GeSn thin film starts to crystallize at 350 °C, in agreement with *ex-situ* TEM results. The grains grow with thermal annealing. It should be noted that a halo ring exists in the diffraction pattern of (c), indicating the existence of molten Sn.

Structural evolution during the cooling process is shown in Fig. 10. These bright-field images were taken from almost the same region as in Fig. 9. As observed in Fig. 9(c), the selected-area electron diffraction pattern recorded at 350 °C consists of discontinuous spot rings and a continuous diffuse halo ring (Fig. 10(a)). The intensity of the halo ring increases with cooling (Fig. 10(b)), corresponding to the development of short-range order. Interestingly, the halo ring is observed at 100 °C (Fig. 10(c)), suggesting that the liquid phase remains below the eutectic temperature of the Ge-Sn binary system. The mechanism of stabilization of liquid Sn below its melting temperature is not well understood yet, but it has been reported that the eutectic point of alloy nanoparticles can be suppressed much faster than the melting point of pure components with decreasing particle size.[29] Based on this result, we speculate that a small amount of Ge atoms is incorporated in the segregated Sn.

The diffraction spots from Sn are not observed in Figs. 10(a)–10(c), while they appear after cooling to room temperature (Fig. 10(d)). The formation of Sn crystallites is in agreement with the results of *ex-situ* observations described

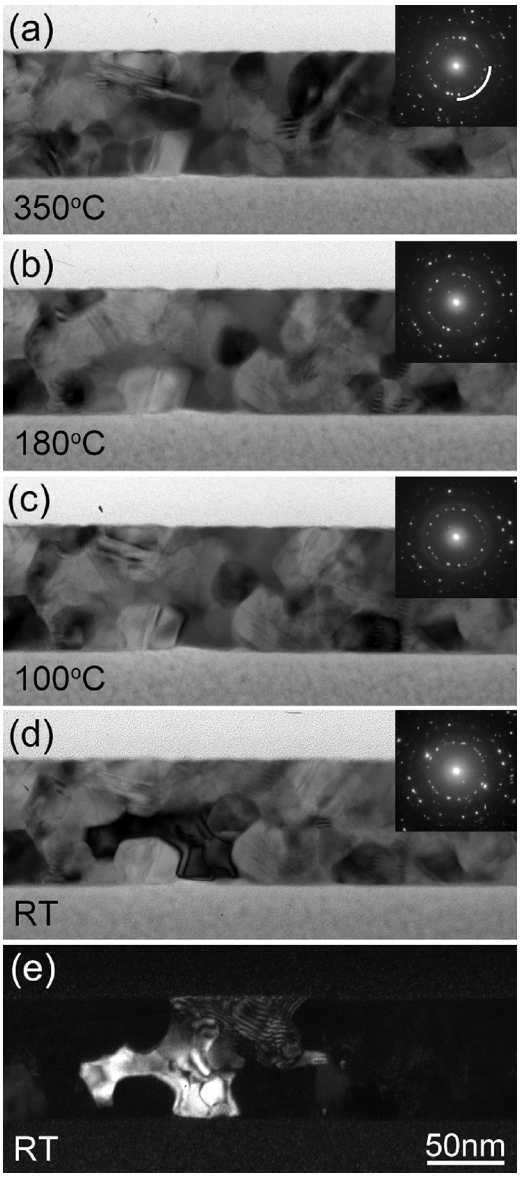

FIG. 10. *In-situ* TEM observations of structural evolution of GeSn during the cooling process. (a) 350 °C, (b) 180 °C, (c) 100 °C, and (d) room temperature. (e) Dark-field TEM image taken at room temperature using the Bragg spot of β-Sn. A halo ring exists in the diffraction pattern in (a-c), indicating the existence of molten Sn.

above. Figure 10(e) shows a dark-field image taken using the Bragg spot of β-Sn, and the Sn precipitate is clearly observed. The region corresponding to Sn becomes dark in the bright-field image at room temperature (Fig. 10(d)), while the contrast is weak in Fig. 10(c). (Note that a faint diffraction contrast probably originates from the matrix overlapped with the precipitates.) This indicates the melting of Sn at 100 °C, consistent with the electron diffraction results.

To examine the structural changes in amorphous GeSn during thermal annealing, an atomic pair-distribution function analysis was performed by the quantitative analysis of nano-beam electron diffraction intensities taken by a convergent beam with a diameter of ~20 nm. Figure 11(a) shows the reduced interference functions, $F(Q)$, of amorphous GeSn obtained by *in-situ* observations. Very weak intensity profiles up to scattering angles as high as $Q = 220\,\mathrm{nm}^{-1}$ are recorded well above the background intensity level of the imaging plate. (The scattering vector is defined as $Q = 2\pi/d = 4\pi\sin\theta/\lambda$, where θ is the half-scattering angle, λ is the electron wavelength, and $1/d$ is the distance in the reciprocal-lattice space.) The intensity of the first peak at $\sim 20\,\mathrm{nm}^{-1}$ suddenly decreases at 250 °C during the heating process, while it increases at 250 °C during the cooling process. The diffraction intensities are affected by the atomic configuration; therefore, a change suggests the occurrence of structural alterations in amorphous networks.

By Fourier transforming the $F(Q)$, atomic pair-distribution functions, $g(r)$, as a function of annealing temperature were obtained (Fig. 11(b)). Interatomic distances in Ge (lattice parameter: $a = 0.5658$ nm) and α-Sn ($a = 0.6493$ nm) are indicated by thick and dotted lines, respectively. Broken lines indicate the Ge-Sn bond length, extracted by averaging the atomic distance of Ge-Ge and Sn-Sn in the diamond structure. For comparison, the interatomic distances in β-Sn ($a = 0.5832$ nm, $c = 0.3181$ nm) are also indicated by thin lines. Prominent first and second peaks appear at 0.25 and 0.40 nm, respectively, which correspond to the Ge-Ge atomic distance. This result is reasonable because Ge is a dominant element in the present specimens. The first peak has a tail in the high-r region, suggesting the formation of Ge-Sn and Sn-Sn atomic pairs. It should be noted that small humps exist between the first and second peaks (0.31 nm), and they are attributed to β-Sn-like bonds.

A notable change is observed in the second coordination shell at annealing temperatures above the eutectic point. The peak corresponding to the Ge-Ge correlation decreases, and as a consequence, the second peak becomes flat. We have recently examined structural changes in amorphous Ge using atomic pair-distribution function analysis and found that only a change in the peak height occurs.[30,31] On the other hand, the peak shape corresponding to the second nearest neighbors is drastically changed in Fig. 11(b). Such a change is not observed in amorphous Ge; therefore, it is concluded that the second nearest neighbor Ge atoms were replaced by Sn atoms above the eutectic temperature. The second coordination shell returns to its original shape at nearly eutectic temperatures during cooling. In contrast to the crystallized GeSn, a supercooled state was not confirmed. This means that an amorphous-to-amorphous phase transformation associated with the rearrangement of Sn atoms occurs prior to crystallization, and the structural changes in amorphous networks are reversible with respect to temperature. It should be noted that the humps between the first and second main peaks decrease in the $g(r)$ obtained after thermal annealing. The Sn atoms segregate to the surface and interface in annealed GeSn thin films, as described above. Atomic pair-distribution functions were obtained from the central region of the thin film, confirming that the decrease in the humps is consistent with the reduction of Sn concentration.

To confirm the validity of the present *in-situ* results, we also examined the amorphous structures of GeSn by *ex-situ* TEM observations. Figure 12 shows atomic pair-distribution functions of as-deposited specimens and those annealed at 350 °C. These profiles were extracted from the diffraction patterns recorded at room temperature. It should be noted

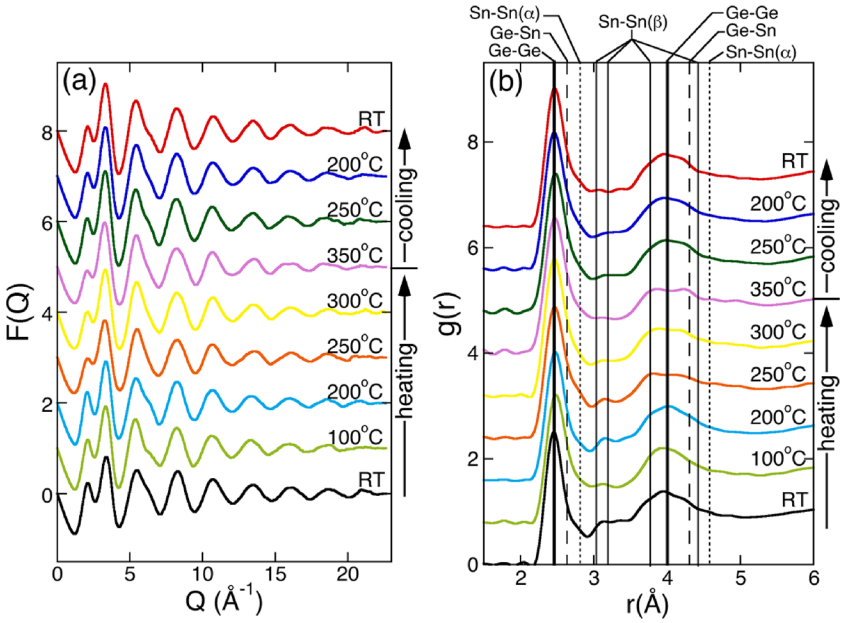

FIG. 11. (a) Reduced interference functions of GeSn as a function of annealing temperature. These data were taken from the same region of the specimen. (b) Atomic pair-distribution functions obtained by the Fourier transform of (a). Interatomic distances of crystalline Ge, GeSn, and Sn are denoted by vertical lines.

that the peak height is affected by the specimen thickness along the electron incidence direction, and therefore only the peak position can be discussed here. The electron diffraction patterns are taken under nearly parallel beam conditions; therefore, the spatial resolution of Fig. 12 is better than that of Fig. 11(b). As a consequence, the peaks from β-Sn-like atomic pairs are clearly separated in the profile of the as-deposited specimen. The features of the $g(r)$ are in good agreement with those of the $g(r)$ obtained at room temperature in Fig. 11(b), suggesting that the present *in-situ* results reproduce the actual structural changes during thermal annealing.

IV. CONCLUSIONS

We prepared amorphous GeSn thin films with Sn concentrations beyond the solubility limit of the *bulk* Ge-Sn binary system and examined the behavior of Sn atoms during thermal annealing using XPS, GIXRD, and (S)TEM. In the as-deposited specimens, Sn atoms were homogeneously distributed in the amorphous matrix. Most of the Sn atoms remain after thermal annealing, although the annealing temperature is much higher than the eutectic point of the Ge-Sn binary system. An amorphous-to-amorphous phase transformation resulting from the rearrangement of Sn atoms at the second coordination shell occurred between 200 °C and 250 °C. The GeSn thin film started to crystallize at 350 °C, and remarkable recrystallization occurred at temperatures above 400 °C. With increasing annealing temperature, Sn atoms were ejected from the crystallized GeSn matrix and a significant Sn segregation was detected in the specimen annealed at >475 °C. The specimens were partially melted because of the aggregation of Sn atoms. It was found that the molten Sn remains below the eutectic temperature during the cooling process. The formation of the supercooled liquid is attributed to the slight incorporation of Ge atoms in Sn. Finally, the molten Sn transformed to β-Sn at ambient temperature.

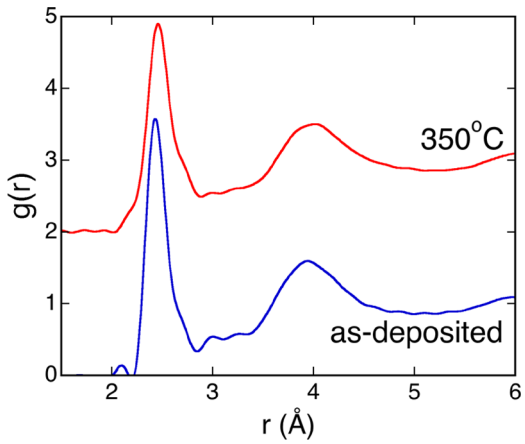

FIG. 12. Atomic pair distribution functions of as-deposited GeSn specimens and those annealed at 350 °C. The diffraction patterns were taken at room temperature. The shape of peaks is almost the same between pre- and post-annealed specimens. The humps from β-Sn-like bonding become small after annealing, suggesting a slight reduction in the Sn concentration.

ACKNOWLEDGMENTS

We are grateful to Ms. Kazuyo Omura and Mr. Yoshihiro Murakami for the technical support of XPS and GIXRD, respectively, at the Cooperative Research and Development Center for Advanced Materials, Institute of Materials Research (IMR), Tohoku University. STEM observations using a JEM-ARM200F were performed at IMR at Tohoku University in Advanced Characterization Nanotechnology Platform.

[1]For example, see S. Zaima, O. Nakatsuka, N. Taoka, M. Kurosawa, W. Takeuchi, and M. Sakashita, Sci. Technol. Adv. Mater. **16**, 043502 (2015).
[2]R. Roucka, J. Tolle, C. Cook, A. V. G. Chizmeshya, J. Kouvetakis, V. D'Costa, J. Menendez, Z. D. Chen, and S. Zollner, Appl. Phys. Lett. **86**, 191912 (2005).
[3]M. Hansen and K. Anderko, *Constitution of Binary Alloys* (McGraw-Hill, New York, 1958).
[4]R. R. Lieten, S. Decoster, M. Menghini, J. W. Seo, A. Vantomme, and J. P. Locquet, ECS Trans. **50**, 915 (2013).

[5]R. R. Liete, J. W. Seo, S. Decoster, A. Vantomme, S. Peters, K. C. Bustillo, E. E. Haller, M. Menghini, and J. P. Locquet, Appl. Phys. Lett. **102**, 052106 (2013).
[6]K. Toko, N. Oya, N. Saitoh, N. Yoshizawa, and T. Suemasu, Appl. Phys. Lett. **106**, 082109 (2015).
[7]W. Takeuchi, N. Taoka, M. Kurosawa, M. Sakashita, O. Nakatsuka, and S. Zaima, Appl. Phys. Lett. **107**, 022103 (2015).
[8]M. Kurosawa, N. Taoka, M. Sakashita, O. Nakatsuka, M. Miyao, and S. Zaima, Appl. Phys. Lett. **103**, 101904 (2013).
[9]T. Sameshima, Y. Sunaga, and A. Kohno, Jpn. J. Appl. Phys., Part 2 **35**, L308 (1996).
[10]M. Uchida, T. Maeda, R. R. Lieten, S. Okajima, Y. Ohishi, R. Takase, M. Ishimaru, and J.-P. Locquet, Appl. Phys. Lett. **107**, 232105 (2015).
[11]For example, see S. R. Elliott, *Physics of Amorphous Materials*, 2nd ed. (Longman Scientific and Technical, 1990), p. 81.
[12]Y. Hirotsu, M. Ishimaru, T. Ohkubo, T. Hanada, and M. Sugiyama, J. Electron Microsc. **50**, 435 (2001).
[13]M. Ishimaru, I.-T. Bae, Y. Hirotsu, S. Matsumura, and K. E. Sickafus, Phys. Rev. Lett. **89**, 055502 (2002).
[14]M. Naito, M. Ishimaru, Y. Hirotsu, and M. Takashima, J. Appl. Phys. **95**, 8130 (2004).
[15]M. Ishimaru, Nucl. Instrum. Methods Phys. Res., Sect. B **250**, 309 (2006).
[16]M. Ishimaru, A. Hirata, M. Naito, I.-T. Bae, Y. Zhang, and W. J. Weber, J. Appl. Phys. **104**, 033503 (2008).
[17]R. Nakamura, M. Ishimaru, H. Yasuda, and H. Nakajima, J. Appl. Phys. **113**, 064312 (2013).
[18]D. Lei, W. Wang, Z. Zhang, J. Pan, X. Gong, G. Liang, E.-S. Tok, and Y.-C. Yeo, J. Appl. Phys. **119**, 024502 (2016).
[19]A. V. G. Chizmeshya, M. R. Bauer, and J. Kouvetakis, Chem. Mater. **15**, 2511 (2003).
[20]A. Chroneos, Phys. Status Solidi B **244**, 3206 (2007).
[21]A. Chroneos, C. Jiang, R. W. Grimes, U. Schwingenschlögl, and H. Bracht, Appl. Phys. Lett. **94**, 252104 (2009).
[22]H. Tahini, A. Chroneos, R. W. Grimes, and U. Schwingenschlögl, Appl. Phys. Lett. **99**, 162103 (2011).
[23]J. J. Pulikkotil, A. Chroneos, and U. Schwingenschlögl, J. Appl. Phys. **110**, 036105 (2011).
[24]R. Nakamura, T. Shudo, A. Hirata, M. Ishimaru, and H. Nakajima, Scr. Mater. **64**, 197 (2011).
[25]R. Nakamura, M. Ishimaru, A. Hirata, K. Sato, M. Tane, H. Kimizuka, T. Shudo, T. J. Konno, and H. Nakajima, J. Appl. Phys. **110**, 064324 (2011).
[26]R. Nakamura, M. Ishimaru, K. Sato, K. Tanaka, H. Nakajima, and T. J. Konno, J. Appl. Phys. **114**, 124308 (2013).
[27]Z. H. Cao, P. Liu, X. K. Meng, S. C. Tang, and H. M. Lu, Appl. Phys. A **94**, 393 (2009).
[28]R. R. Lieten, C. Fleischmann, S. Peters, N. M. Santos, L. M. Amorim, Y. Shimura, N. Uchida, T. Maeda, S. Nikitenko, T. Conard, J.-P. Locquet, K. Temst, and A. Vantomme, ECS J. Solid State Sci. Technol. **3**, P403 (2014).
[29]J.-G. Lee and H. Mori, Thin Solid Films **546**, 453 (2013).
[30]M. Okugawa, R. Nakamura, M. Ishimaru, K. Watanabe, H. Yasuda, and H. Numakura, J. Appl. Phys. **119**, 214309 (2016).
[31]M. Okugawa, R. Nakamura, M. Ishimaru, H. Yasuda, and H. Numakura, J. Appl. Phys. **120**, 134308 (2016).